Turkish Journal of Electrical Engineering & Computer Sciences

http://journals.tubitak.gov.tr/elektrik/

Research Article

Turk J Elec Eng & Comp Sci
(2019) 27: 316 – 329

doi:10.3906/elk-1712-186

Fuzzy-logic-based robust speed control of switched reluctance motor for low and high speeds

Zeki OMAÇ*
Department of Electrical and Electronics Engineering, Faculty of Engineering, Munzur University, Tunceli, Turkey

Received: 14.12.2017 • **Accepted/Published Online:** 30.08.2018 • **Final Version:** 22.01.2019

Abstract: Switched reluctance motor (SRM) is operated at high magnetic saturation to generate large torque. The flux linkage of SRM is a nonlinear function with phase current and rotor position because of the high magnetic saturation. Also, the performance of the speed controller for the SRM driver system can be negatively affected by noise, disturbances, and inertia of load torque. Therefore, the fuzzy speed controller for the SRM driver system was developed in this study. In addition, a dynamic model of SRM was simulated in Matlab/Simulink software. Based on the results obtained in this study, the speed of the SRM was controlled over a wide range of speeds including low and high speeds by the fuzzy speed controller. Furthermore, in simulation, the rotor speed was simulated depending on the reference speed. Moreover, the speed of the SRM was experimentally tested using the DS1103 Ace kit. Finally, simulation results were compared with experimental results and they were found to be consistent with each other.

Key words: Fuzzy logic control, switched reluctance motor

1. Introduction

In recent years, induction motor (IM), permanent magnet synchronous motor (PMSM), and switched reluctance motor (SRM) have received increasing attention in industrial applications. Among these motors, SRM stands out with its simple and rugged structure [1–4]. In addition, there are no magnets and windings in the rotor of SRM and there are only windings on the stator poles. Furthermore, the stator and rotor are manufactured from low-cost silicon sheets with doubly salient structure. Therefore, SRM is robust and capable of performing in harsh operating conditions and high temperatures.

SRMs have a number of industrial applications such as servomotor drives, household appliances, electric vehicles, electric aircraft, wind turbines, and air conditioning fans due to fault tolerance, low inertia, low maintenance cost, high efficiency, high torque generating capability, and easy speed control [5–9]. However, due to double salient structure of the stator and rotor poles, the ripple in electromagnetic torque is produced in the SRM [10]. This motor also has acoustic noise and vibration issues because of radial forces [11]. In addition, the nonlinear variation of torque generation and inductance change depending on phase current and rotor position makes dynamic modeling of SRM and high-performance speed control difficult [12]. Although the control for SRM drivers are not easy due to the effect of back electromotive force (EMF); recent developments in power electronics, digital signal processors, and sensors have facilitated the control of SRM drivers over a wide range of speeds. Hence, several current control approaches including ramp comparison control with

*Correspondence: zomac@munzur.edu.tr

constant switching frequency, hysteresis control, and adaptive sliding current control have been developed [3]. Recently, proportional–integral (PI) and proportional–integral–derivative (PID) controllers used in industrial applications without complicated mathematical model have been developed for SRM derivers. It is also possible to get an excellent speed response at control of the SRM for a constant speed with good settings of parameters of PI and PID controllers. In [3], the winding current of the SRM was controlled using the PI controller by the pulse width modulation technique (PWM) and the current controller dynamically controls turn on and turn off angles depending on the current error using the back EMF observer for robust speed control has been developed. Similarly, a fast, stable, noise-free digital PWM current controller is designed for the SRM driver [13]. Likewise, a study [14] proposed a constant gain PI current controller that compensates for the disturbance effect of back EMF under different operating conditions using the linear model of SRM with a simple model. Moreover, a novel PI speed control [15] and current control [16] by using a digital signal processor for SRM drives were designed to reduce the radial force acting on the stator poles and they had a wide speed range. On the other hand, the performance of a PI or PID controller can be considerably deteriorated by altered operation conditions, such as high magnetic saturation.

Intelligent control methods including fuzzy logic control (FLC) can be used for better performance when the exact analytical model of the controlled system is changeable or complex to be characterized. They try to imitate and learn the experience of the human expert to gain sufficient achievement for the controlled plant. Translating linguistic control rules into practical operation mechanism also makes FLC one of the most powerful tools appropriate for controller design while the plant is hard to model mathematically because of its complexity, nonlinearity, and/or inaccuracy. Therefore, the applicability of FLC was reported in several studies [17–21]. In [17], a fuzzy controller acting as a PI controller with self-tuning gain was used for an SRM driver system and a simple controller was developed by reducing the number of sets in membership functions without losing anything in system performance and stability. In addition, the new adaptive fuzzy cerebellar model articulation controller (CMAC) was implemented on an SRM system [18]. Similarly, a fuzzy logic controller was developed for speed control of an SRM [19]. Likewise, the Takagi–Sugeno–Kang (TSK)-type fuzzy controller was used in the speed control of SRM [20]. Besides, the switched reluctance external rotor motor drive with the closed-loop rotor speed control for a fan in air conditioner was implemented using a fuzzy logic algorithm [21]. Comparative analyses between PI controller and fuzzy logic controller were performed to overcome the shortcomings of the PI controller [22–31].

In this study, a fuzzy logic controller was developed and used to achieve a wide range of speeds, including low and high speeds for the SRM derive system. Also, the success of the fuzzy-logic-based robust speed-controlled driver was experimentally verified.

2. Switched reluctance motor

In SRM, the stator and the rotor are manufactured from thin silicon steel sheets with a salient pole structure. The windings are placed on the stator poles and fed with the direct voltage. A phase-coil voltage equation of the SRM is given as follows:

$$v_j = R_j i_j + \frac{\lambda_j(\theta_r, i_j)}{dt}, j = a, b, c, \tag{1}$$

where v_j is the stator phase voltage, i_j is the stator phase current, R_j is the stator phase winding resistance, λ_j is the stator phase flux linkage, θ_r is the rotor position, and j is indices of a, b, c phases. Mutual inductance

between the phases can be neglected if the phases are energized in sequence alone. In this case, for a phase flux, the relationship can be written as in Eq. (2):

$$\lambda_j = L_{jj}(\theta_r, i_j) i_j, j = a, b, c, \tag{2}$$

where L_{jj} is the self-inductance of a phase winding. Torque equation can be written for induced in rotor as in Eq. (3):

$$T_e = \frac{1}{2} \sum_{j=a}^{b,c} i_j^2 \frac{L_{jj}}{\theta_r}. \tag{3}$$

Motion equation of SRM is as in Eq. (4):

$$T_e = J \frac{d\omega_r}{dt} + B\omega_r + T_L, \tag{4}$$

where T_e is the induced electromagnetic torque, J is the inertia, B is the viscous frictional coefficient, T_L is the load torque, and ω_r is the rotor speed.

Model of SRM has a critical role in determining performance. To obtain the characteristics of the SRM, there are many methods, such as the magnetic equivalent circuit, the finite element method (FEM), and the measurement method, which have different advantages and disadvantages [32]. A motor phase winding current was applied as 2.78 A, 3.71 A, 4.64 A, 5.57 A, and 6.5 A, respectively. Inductance and torque values were calculated for each position by rotating the rotor position by one degree mechanical angle.

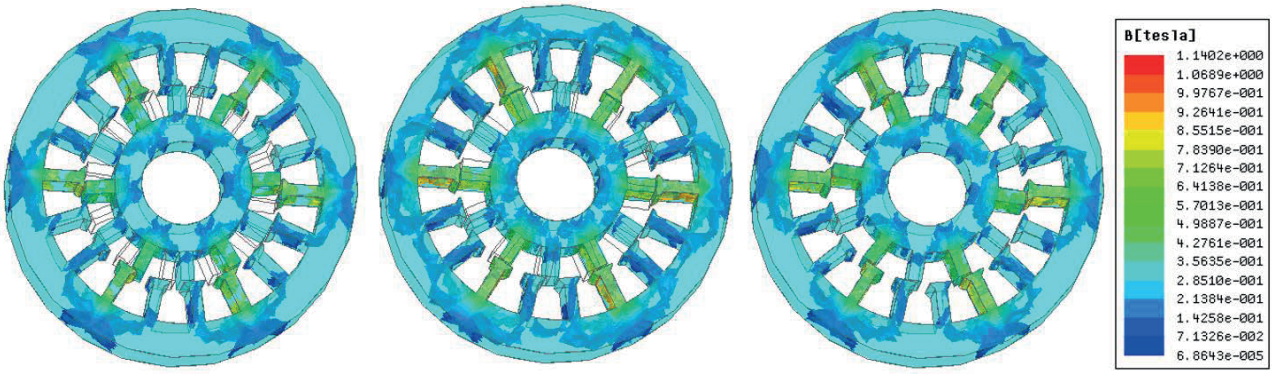

Figure 1. Field disturbances of SRM for different rotor positions in nominal current.

Three-dimensional (3-D) motor geometry by using Ansys/Maxwell 3-D software was used to improve the accuracy of calculations. Ansys/Maxwell 3-D software is also a packaged software that allows magnetic analysis of electric machines in 3-D FEM. Field disturbances are shown in Figure 1 for 6.5 A nominal phase current. Figures 2a and 2b show the phase coil inductance values and torque values, respectively, that were calculated from the FEM with the Ansys/Maxwell 3-D software. As a result of the magnetic analysis, it was observed that torque value increases in the region where inductance increases, and that magnetic saturation increases at pole feet in aligned position in nominal phase current.

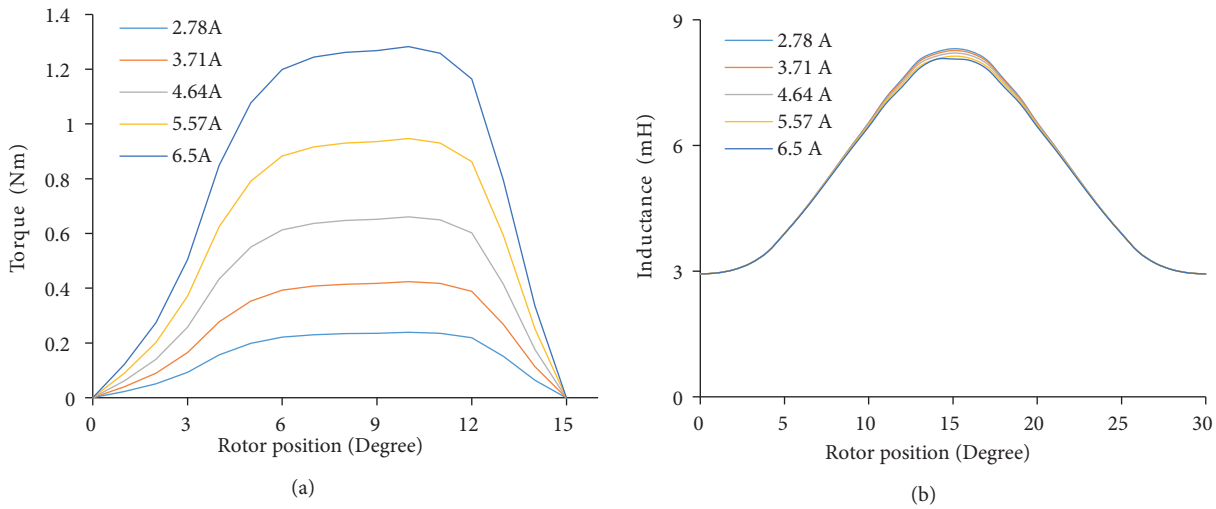

Figure 2. For different values of phase current and rotor position one phase; (a)Torque graphs, (b)Inductance graphs.

3. Fuzzy logic controller design

A fuzzy controller, as shown in Figure 3, includes parts such as fuzzification, inference mechanism, rule base, and defuzzification. The fuzzy controller controls the output of a system according to the input reference. The input and output of the fuzzy controller consist of crisp sets. The fuzzification block converts the crisp inputs to fuzzy sets, and the defuzzification block converts fuzzy sets to crisp outputs [17,33]. Let us consider a discrete-time controller with two inputs and one output. The error (e) and change of error (Δe) are used as input variables, as in Figure 4.

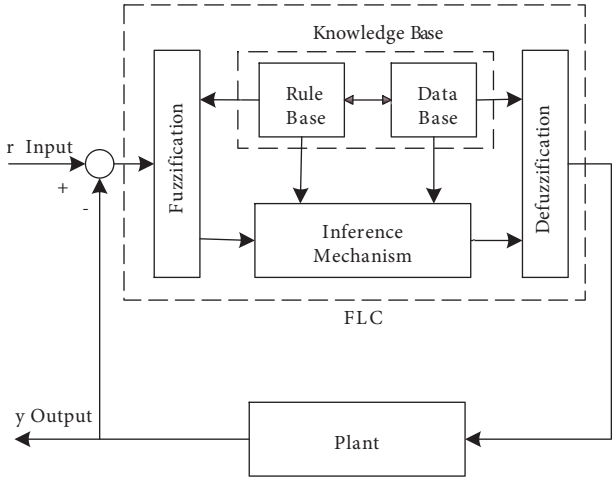

Figure 3. Internal structure of a fuzzy logic controller.

$$e(k) = r(k) - y(k), \tag{5}$$

$$\Delta e(k) = e(k) - e(k-1), \tag{6}$$

where r is the input control signal and y is the system output. The k and k-1 indices show the current and previous state of the system, respectively. The membership functions of e and Δe input, and the Δu

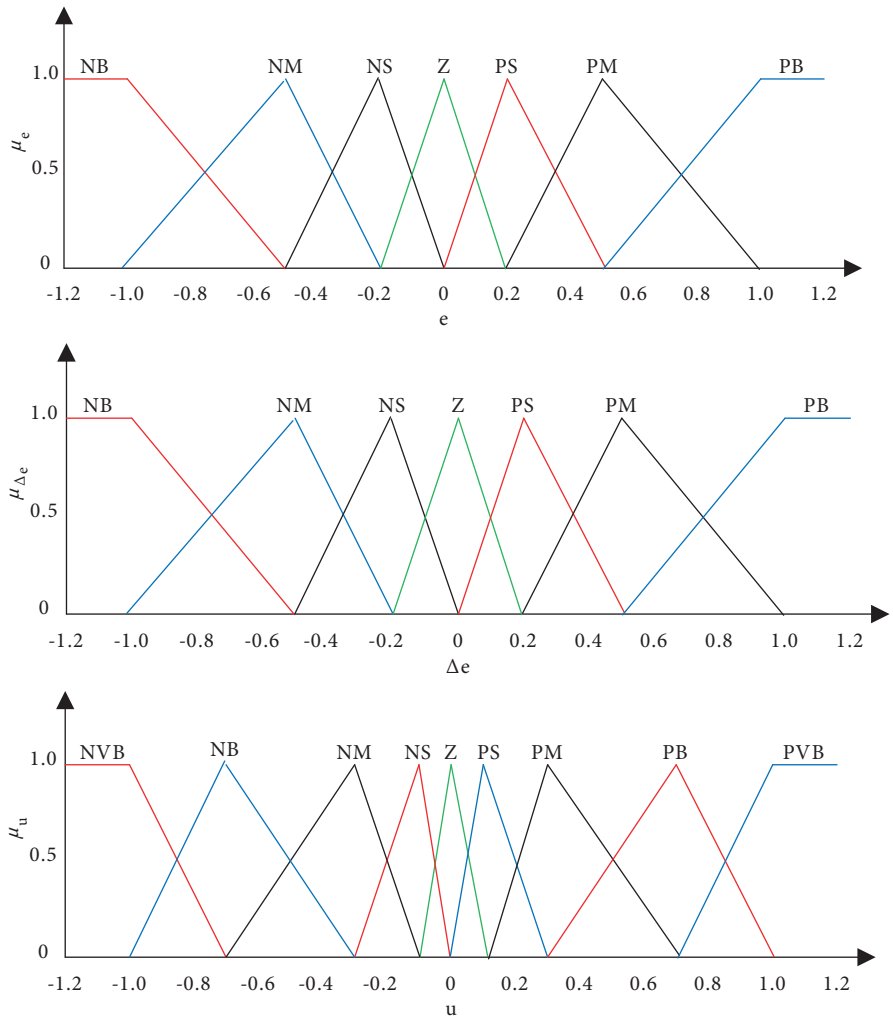

Figure 4. Membership functions.

output variables of the fuzzy controller are normalized in the interval $[-1.2, 1.2]$, as shown in Figure 4. The abbreviations NVB, NB, NM, NS, Z, PS, PM, PB, and PVB show linguistic expressions: negative very large, negative large, negative medium, negative small, zero, positive small, positive medium, positive large, and positive very large, respectively. G_e, $G_{\Delta e}$, and $G_{\Delta u}$ are the coefficients used in the normalization of the input and output variables. The rule base defines the rules between e and Δe input variables, and Δu output variable. The rule base that calculates the Δu controller output based on the inputs e and Δe is shown in Table 1.

For example, Rule Δu: if e is NB and Δe is NB then Δu is NVB.

The fuzzy logic speed control block diagram of the SRM driver is shown in Figure 5. In this diagram, the rotor speed is subtracted from the reference speed and the resulting speed error and change of speed error are used as input data in the fuzzy speed controller. The reference current signal obtained at the output of the speed controller is compared with the phase currents. The current error is passed through a PI current controller to generate PWM control signals of the phases. The rotor position information from the encoder is processed in the commutation block to determine the turn on and turn off angles of the phases.

The fuzzy speed controller detail is shown in Figure 6, where G_e, $G_{\Delta e}$, and G_u are normalization factors

Table 1. Rule base for output function.

e / Δe	NB	NM	NS	ZE	PS	PM	PB
NB	NVB	NVB	NVB	NB	NM	NS	ZE
NM	NVB	NVB	NB	NM	NS	ZE	PS
NS	NVB	NB	NM	NS	ZE	PS	PM
ZE	NB	NM	NS	ZE	PS	PM	PB
PS	NM	NS	ZE	PS	PM	PB	PVB
PM	NS	ZE	PS	PM	PB	PVB	PVB
PB	ZE	PS	PM	PB	PVB	PVB	PVB

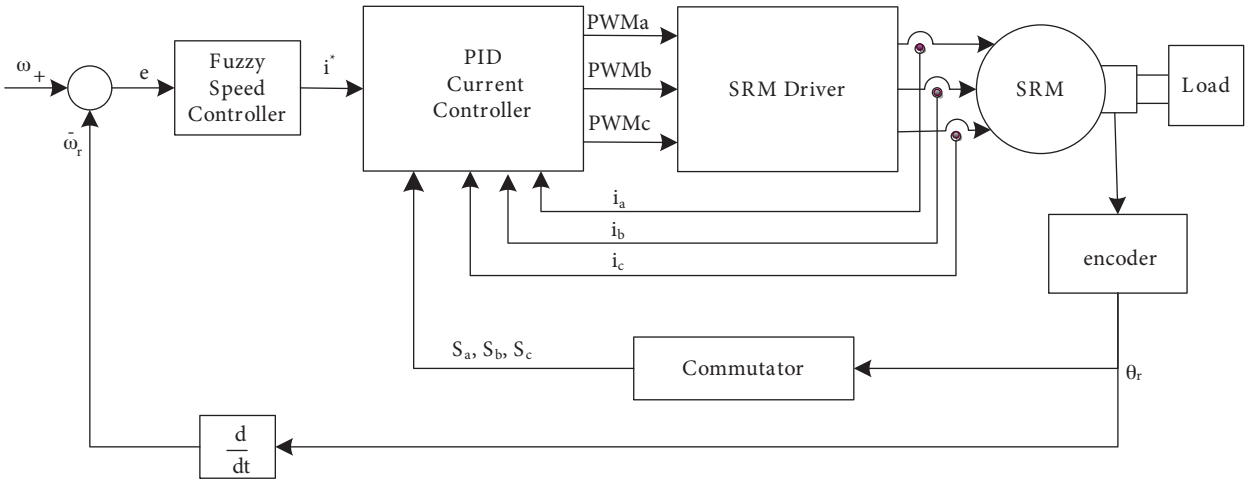

Figure 5. SRM's fuzzy logic speed control block diagram of driver.

of the error, change of error, and output function, respectively. For constants used in normalization, $G_e = 0.024$, $G_{\Delta e} = 1$, and $G_{\Delta u} = 1000$ values are determined.

4. Experimental setup and results

SRM's fuzzy logic speed control model was built in Matlab/Simulink software. Fuzzy logic speed controller was tested on an SRM driver to determine efficiency and accuracy of the proposed fuzzy logic speed controller. The experimental setup block diagram is shown in Figure 7a, and the photograph is shown in Figure 7b. Three-phase asymmetric bridge power converter was used in SRM driving. In this circuit, there were two switches and two flywheel diodes in each phase. Insulated-gate bipolar transistors (IGBT) were chosen as main switches. Fast recovery diodes were adopted as flywheel diodes. The rotor position and speed information was measured via an incremental encoder connected to the rotor shaft. Phase currents were sensed with three Hall Effect current transducers. DS 1103 Ace-kit containing the DS1103 R & D control board (dSPACE GmbH LLC, Paderborn, Germany) was used for system control. The DS1103 R & D control board was designed as a high-speed digital controller. The board included Texas Instruments TMS320F240 microcontroller (Dallas, TX, USA) as a slave digital signal processor (DSP) and was equipped with 32 MB boot flash, 96 MB DRAM, 20 analog-to-digital converters, eight 16-bit digital-to-analog converters, three phase PWM outputs and four single PWM outputs, 20 bit digital I/O, incremental encoder converter.

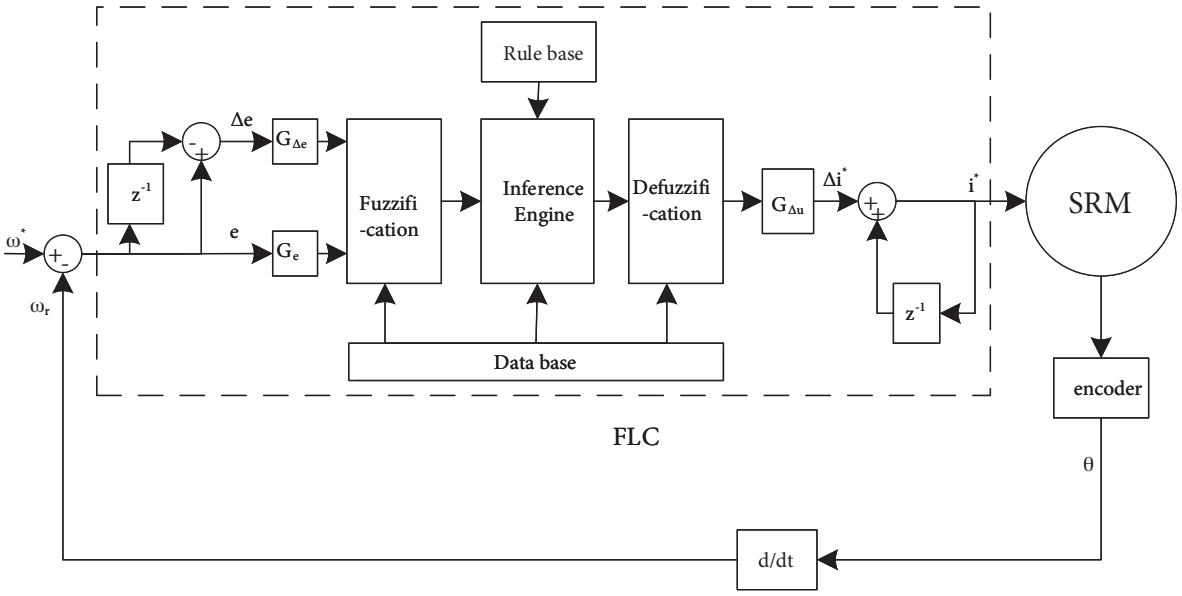

Figure 6. Details of fuzzy speed controller.

The communication between computer and the board, which was inserted in a dSPACE expansion box, is provided via fiber optic cable over ISA-bus extension (DS817). Fuzzy logic speed control model of the SRM was prepared in Matlab/Simulink on computer, and DS1103 controldesk software produced codes to be processed in real time. The switching frequency and sampling frequency were selected as 15 kHz. SRM parameters used in simulation are given in Table 2.

Table 2. SRM parameters.

Constant	Value
Voltage	100 V
Number of stator poles	18
Number of rotor poles	12
One-phase winding resistance	2.6 Ω
Coefficient of friction	0.0055 Nm/(rad/s)
Moment of inertia	0.00695 Kgm^2
Load torque	1.0 Nm

It was observed that rotor speed caught and stabilized with the reference speed in a short time. Graphs of rotor speed and phase currents obtained by simulation and measured by experimental for different reference speed values and without load are shown in Figures 8a–8f using PI speed controller, and fuzzy speed controller.

In this case, graphs of rotor speed and phase currents measured without load, respectively. In both graphs, reference speeds were set as time interval 0–1 s $\omega_{ref} = 50$ rad/s, time interval 1–2 s $\omega_{ref} = 100$ rad/s, time interval 2–3 s $\omega_{ref} = 50$ rad/s, time interval 3–4 s $\omega_{ref} = -50$ rad/s, time interval 4–5 s $\omega_{ref} = -100$ rad/s, time interval 5–6 s $\omega_{ref} = -50$ rad/s, time interval 6–7 s $\omega_{ref} = 50$ rad/s, respectively. The respond of rotor speed (ω) was investigated based on changes in the reference speeds.

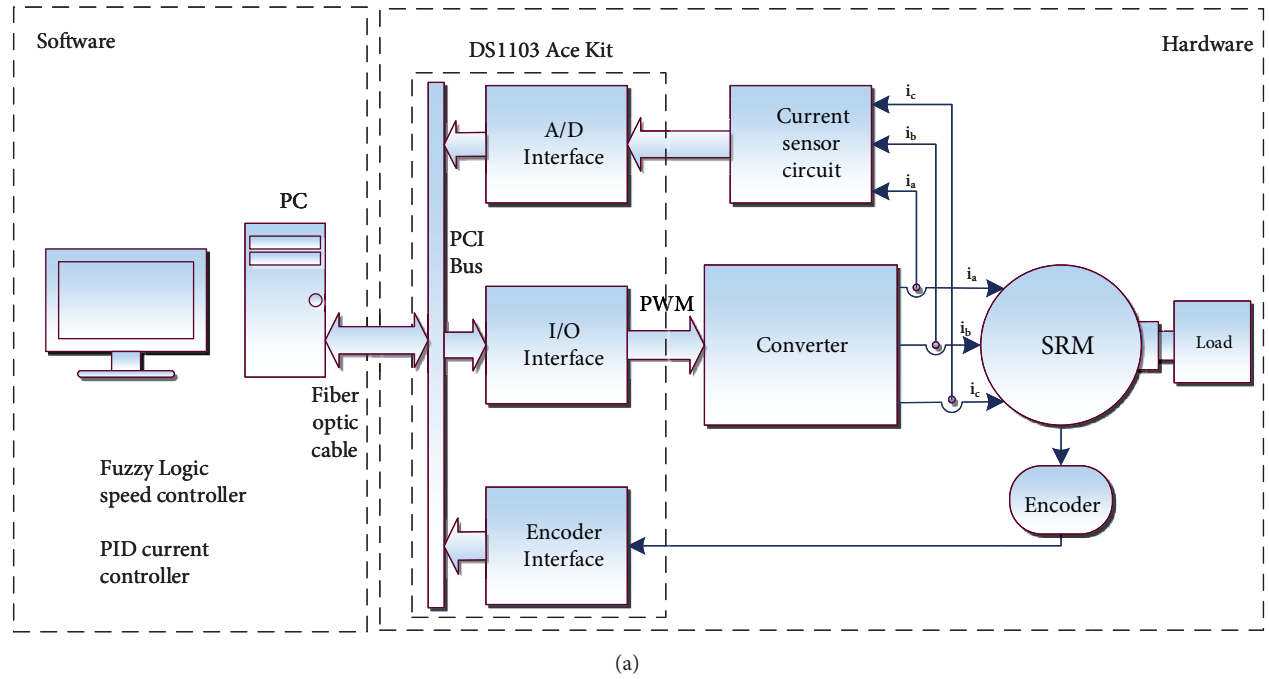

(a)

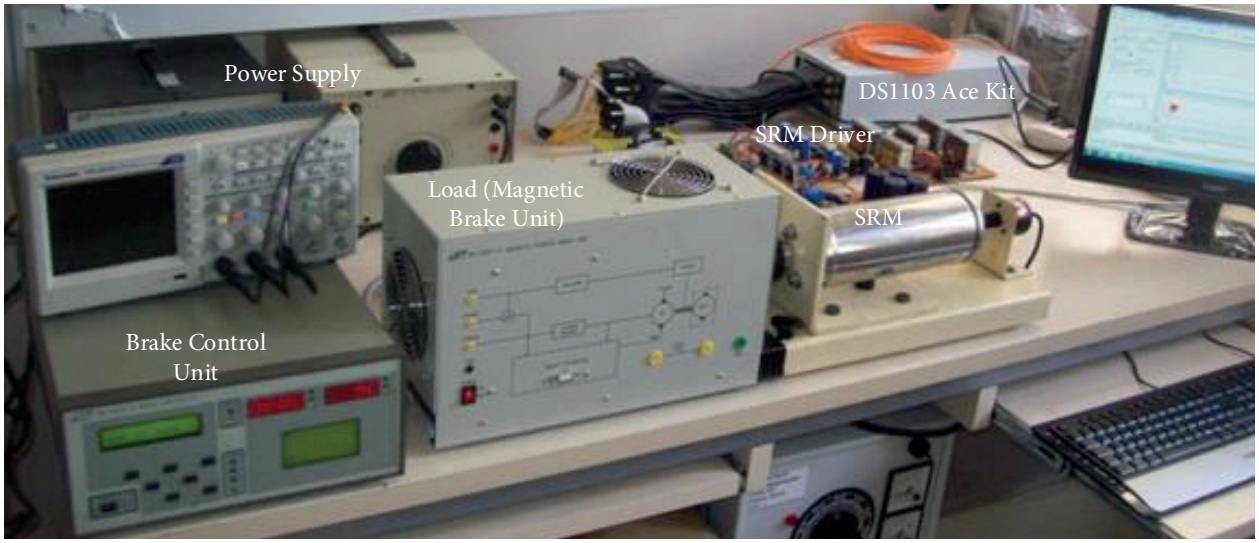

(b)

Figure 7. Experimental setup; (a) Block diagram, (b) Photograph.

The motor was loaded with T_L=1.0 Nm of load torque to measure the speed of rotor under load. Experimental results and simulation results are given in Figures 9a–9f for different reference speed values using PI speed controller, and fuzzy speed controller. The results showed that rotor speed accurately tracks changes in reference speed. In addition, they displayed that instantaneous large current pulsations occur in phase currents graphs where reference speed step value increases.

Simulation and experimental results of rotor speed at different reference speeds in unloaded state at low speed are given in Figures 10a–10f using PI speed controller, and fuzzy speed controller. In simulation, while

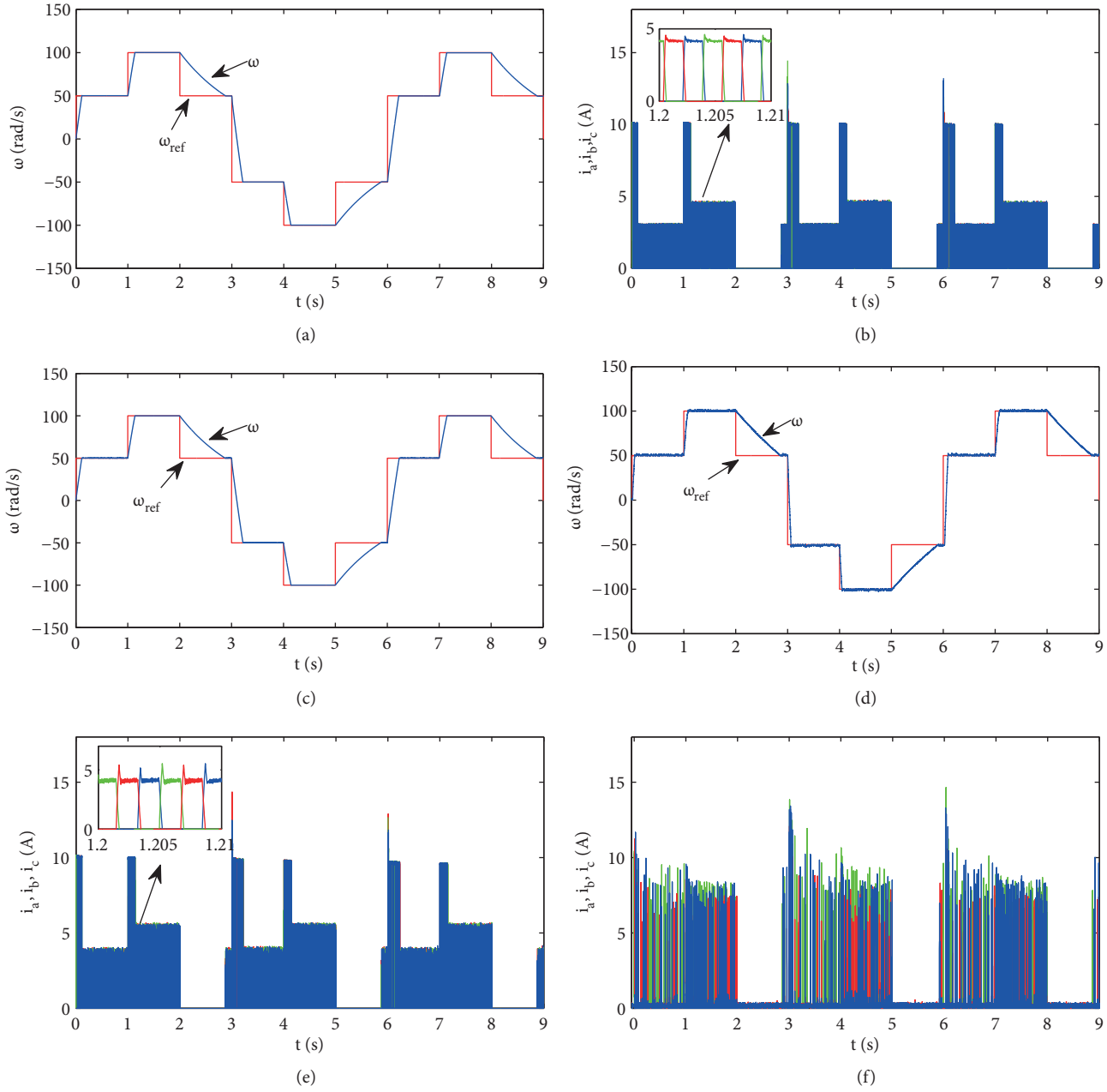

Figure 8. Simulation results were obtained and experimental results were measured for different reference speeds without load, (a) Simulation rotor speed with PI speed controller, (b) Simulation phase currents graphs with PI speed controller, (c) Simulation rotor speed with fuzzy speed controller, (d) Experimental rotor speed with fuzzy speed controller, (e) Simulation phase currents graphs with fuzzy speed controller, (f) Experimental phase currents graphs with fuzzy speed controller.

the rotor speed followed the reference speed properly, experimentally the rotor speed graph consisted of a small ripple. At low speed, the motor was loaded with $T_L = 1.0$ Nm load torque. In the loaded case, simulated results and experimental results of rotor speed at different reference speeds are given in Figures 10b, 10d, and 10f using PI speed controller, and fuzzy speed controller. In simulation, while the rotor speed followed the reference speed properly, experimentally the rotor speed graph consisted of a small ripple.

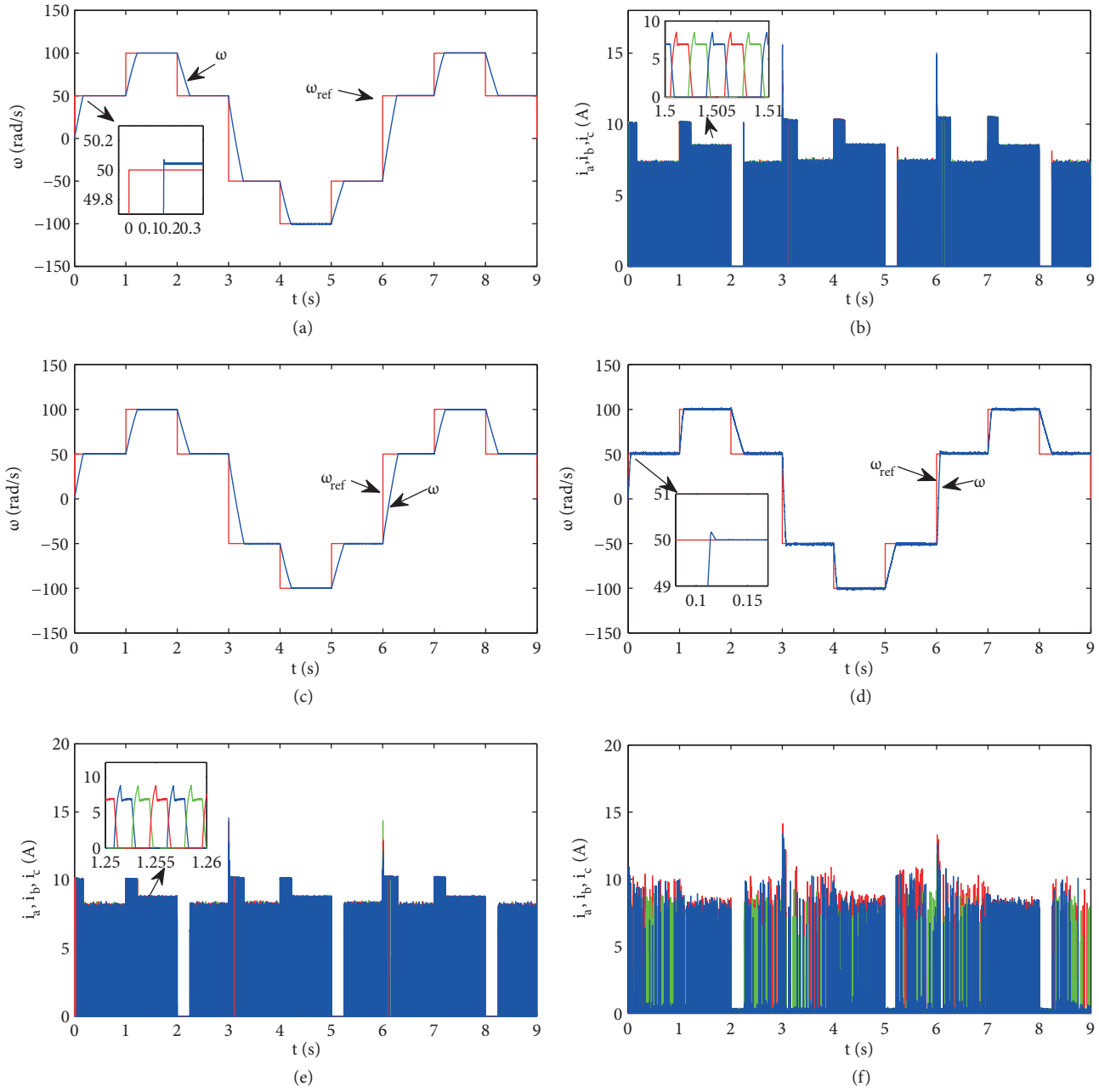

Figure 9. For different reference speeds and for $T_L = 1.0$ Nm load torque (a) Simulation rotor speed with PI speed controller, (b) Simulation phase currents graphs with PI speed controller, (c) Simulation rotor speed with fuzzy speed controller, (d) Experimental rotor speed with fuzzy speed controller, (e) Simulation phase currents graphs with fuzzy speed controller, (f) Experimental phase currents graphs with fuzzy speed controller.

Besides, in the case of the high-speed fuzzy speed controller installed ($T_L = 1.0$ Nm), the experimentally measured speed results are shown in Figure 11a and the phase currents graph is shown in Figure 11b. At high speed, a smooth and steady speed response was obtained from the fuzzy logic speed controller.

The performance of the SRM driver with robust fuzzy controller was analyzed and compared with classical PI controller. At no-load and load conditions, response parameters such as rise time, peak overshoot, settling

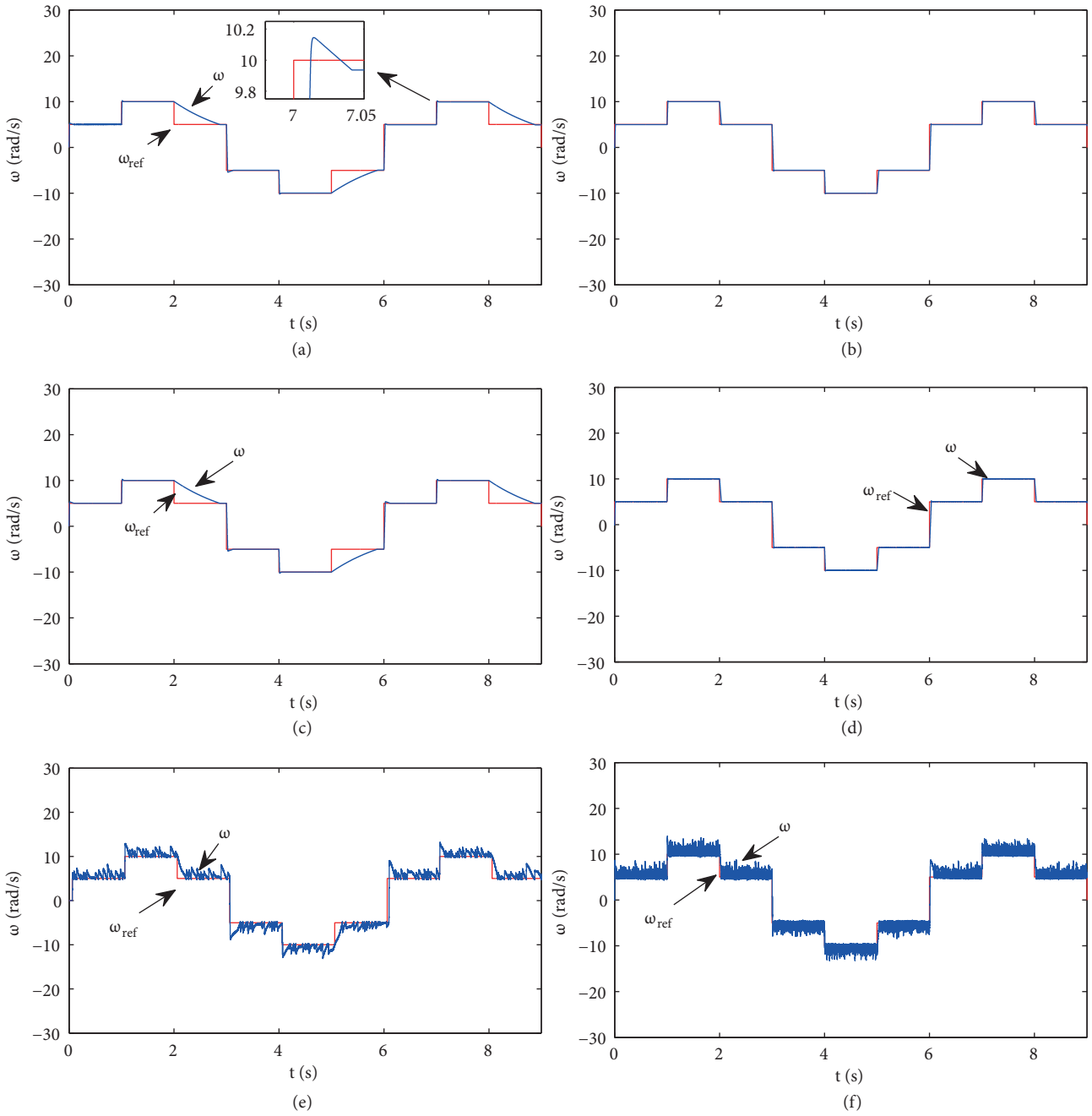

Figure 10. For different reference speeds at low speed, (a) Simulation rotor speed with PI speed controller without load, (b) Simulation rotor speed with PI speed controller for $T_L = 1.0$ Nm load torque, (c) Simulation rotor speed with fuzzy speed controller without load, (d) Simulation rotor speed with fuzzy speed controller for $T_L = 1.0$ Nm load torque,(e) Experimental rotor speed with fuzzy speed controller without load, (f) Experimental rotor speed with fuzzy speed controller for $T_L = 1.0$ Nm load torque.

time, steady state error, and percentage of steady state error were compared for the PI and fuzzy controllers and presented in Tables 3 and 4, respectively. Simulation and experimental results showed that the robust fuzzy speed controller of SRM drive system was proved to be superior than the PI speed controller in steady state error.

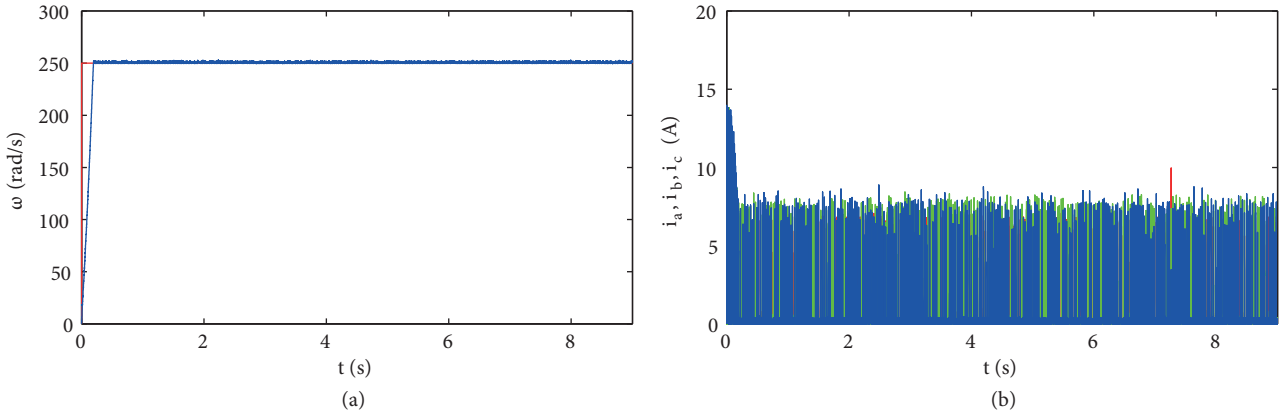

Figure 11. At high speed experimental (a) Rotor speed, (b) Phase currents.

Table 3. Control system parameters for variable reference speeds in no-load condition.

Controller	Reference speed (rad/s)	Rise time (ms)	Peak time (ms)	Peak value (rad/s)	Peak overshoot (%)	Settling time (ms)	Steady state error (rad/s)	Steady state error (%)
PI	50	90	114.6	50.185	0.37	118.3	0.04	0.08
	100	110	136	100.1	0.1	136.8	0.09	0.09
	−50	172	213.25	−50.085	0.170	217.3	0.07	0.14
	−100	110	139	−100.03	0.031	140.1	0.015	0.015
Fuzzy	50	90.6	114.7	50.174	0.348	119.8	0.0005	0.001
	100	110.2	138.8	100.014	0.0146	140	0.0021	0.0021
	−50	179.3	219.8	−50.091	0.184	223.1	0.0005	0.001
	−100	116.1	146.5	−100.03	0.03	147.4	0.005	0.005

Table 4. Control system parameters for variable reference speeds in load condition.

Controller	Reference speed (rad/s)	Rise time (ms)	Peak time (ms)	Peak value (rad/s)	Peak overshoot (%)	Settling time (ms)	Steady state error (rad/s)	Steady state error (%)
PI	50	133.8	169.6	50.069	0.138	170	0.0465	0.093
	100	174.7	221.6	100.149	0.149	222.2	0.129	0.129
	−50	235.9	289.3	−50.3	0.6	291.0	0.25	0.5
	−100	168	215.2	−100.34	0.34	216.5	0.33	0.33
Fuzzy	50	134.7	169.4	50.02	0.04	171	0.01	0.02
	100	177.8	224.8	100.019	0.019	225.5	0.005	0.005
	−50	244.7	298.5	−50.055	0.055	300	0.01	0.01
	−100	178	225.1	−100.03	0.03	225.5	0.02	0.02

5. Conclusion

Based on the results obtained in the present study, the fuzzy logic speed controller was performed at a wide range of speeds, including low and high speeds to control the speed of SRM. The performance of this speed

controller was also simulated using Matlab/Simulink software. In addition, simulation results are obtained for different reference speeds and load torques. To verify accuracy of the simulation results, the experimental results were obtained for these speeds using controller of the DS 1103 Ace kit. For the unloaded and loaded conditions, the experimental results were in excellent agreement with the simulation results. Furthermore, it was experimentally realized that the fuzzy speed controller was robust and not affected by parameter changes and disturbances.

In fuzzy logic controller, optimization algorithms may be applied for fuzzy membership function selection, tuning of fuzzy rule, and input–output scaling factor tuning to reduce response time of the system, and this may be reserved as scope for future work.

Acknowledgment

The author gratefully acknowledges the support of the Munzur University Scientific Research Projects Unit (No: YLTUB011-12).

References

[1] Kiyota K, Kakishima T, Chiba A. Comparison of test result and design stage prediction of switched reluctance motor competitive with 60-kW rare-earth PM motor. IEEE T Ind Electron 2014; 61: 5712-5721.

[2] Yang Z, Shang F, Brown IP, Krishnamurthy M. Comparative study of interior permanent magnet, induction, and switched reluctance motor drives for EV and HEV applications. IEEE T Transp Electrific 2015; 1: 245-254.

[3] Huang HN, Hu KW, Wu YW, Jong TL, Liaw CM. A current control scheme with back emf cancellation and tracking error adapted commutation shift for switched-reluctance motor drive. IEEE T Ind Electron 2016; 63: 7381-7392.

[4] Chiba A, Kiyota K, Hoshi N, Takemoto M, Ogasawara S. Development of a rare-earth-free SR motor with high torque density for hybrid vehicles. IEEE T Energy Conver 2015; 30: 175-182.

[5] Öksüztepe E. In-wheel switched reluctance motor design for electric vehicles by using pareto based multi objective differential evolution algorithm. IEEE T Veh Technol 2017; 66: 4706-4715.

[6] Bartolo JB, Degano M, Espina J, Gerada C. Design and initial testing of a high-speed 45-kW switched reluctance drive for aerospace application. IEEE T Ind Electron 2017; 64: 988-997.

[7] Yıldırım M, Polat M, Öksüztepe E, Omaç Z, Yakut O, Eren H, Kaya M, Kürüm H. Designing in-wheel switched reluctance motor for electric vehicles, In: 16th Power Electronics and Motion Control Conference and Exposition (PEMC'14), 21-24 September 2014; Antalya, Turkey: IEEE. pp 793-798.

[8] Omaç Z, Polat M, Öksüztepe E, Yıldırım M, Yakut O, Eren H, Kaya M, Kürüm H. Design, analysis, and control of in-wheel switched reluctance motor for electric vehicles. Electr Eng 2018; 100: 865-876.

[9] Xue XD, Cheng KWE, Ng TW, Cheung NC. Multi-objective optimization design of in-wheel switched reluctance motors in electric vehicles. IEEE T Ind Electron 2010; 57: 2980-2987.

[10] Kurihara N, Bayless J, Sugimoto H, Chiba A. Noise reduction of switched reluctance motor with high number of poles by novel simplified current waveform at low speed and low torque region. IEEE T Ind Appl 2016; 52: 3013-3021.

[11] Liang X, Li G, Ojeda J, Gabsi M, Ren Z. Comparative study of classical and mutually coupled switched reluctance motors using multiphysics finite-element modeling. IEEE T Ind Electron 2014; 61: 5066-5074.

[12] Santos dos FLM, Anthonis J, Naclerio F, Gyselinck JJC, Auweraer der HV, Góes LCS. Multiphysics NVH modeling: Simulation of a switched reluctance motor for an electric vehicle. IEEE T Ind Electron 2014; 61: 469-476.

[13] Peng F, Ye J, Emadi A. A Digital PWM current controller for switched reluctance motor drives. IEEE T Power Electr 2016; 31: 7087–7098.

[14] Ahmad SS, Narayanan G. Linearized modeling of switched reluctance motor for closed-loop current control. IEEE T Ind Appl 2016; 52: 3146–3158.

[15] Omaç Z, Kürüm H, Selçuk AH. Design, analysis and control of a switched reluctance motor having 18/12 poles. Fırat U Sci Eng J 2007; 3: 339-346.

[16] Omaç Z, Kürüm H, Selçuk AH. Digital current control of switched reluctance motor. Int J Electr Power Eng 2011; 5: 54-61.

[17] Wang SC, Liu YH. A Modified PI-like fuzzy logic controller for switched reluctance motor drives. IEEE T Ind Electron 2011; 58: 1812-1825.

[18] Wang SY, Tseng CL, Chien SC. Adaptive fuzzy cerebellar model articulation control for switched reluctance motor drive. IET Electr Power Appl 2012; 6: 190–202.

[19] Bolognani S, Zigliotto M. Fuzzy logic control of a switched reluctance motor. IEEE T Ind Appl 1996; 32: 814-821.

[20] Tseng CL, Wang SY, Chien SC, Chang CY. Development of a self-tuning TSK-fuzzy speed control strategy for switched reluctance motor. IEEE T Power Electron 2012; 27: 2141-2152.

[21] Chen H, Gua JJ. Switched reluctance motor drive with external rotor for fan in air conditioner. IEEE/ASME T Mechatronics 2013; 18: 1448-1458.

[22] Doğan M, Dursun M. Application of speed control of permanent magnet synchronous machine with PID and fuzzy logic controller. Energy Sci Res 2012; 28: 931-936.

[23] Dursun M, Boz AF, Karabacak M. Sensorless control application of PMSM with a novel adaptation mechanism. Neural Comput Applic 2018; 29: 87-103.

[24] Dursun M, Boz AF, Kale M, Karabacak M. Sensorless speed control of permanent magnet synchronous motor with hybrid speed controller using model reference adaptive system. J Advanced Tech Sci 2014; 3: 24-37.

[25] Premkumar K, Manikandan BV. Adaptive neuro-fuzzy inference system based speed controller for brushless DC motor. Neurocomputing 2014; 138: 260-270.

[26] Premkumar K, Manikandan BV, Kumar CA. Antlion algorithm optimized fuzzy PID supervised on-line recurrent fuzzy neural network based controller for brushless DC motor. Electr Power Comp Syst 2017; 45: 2304-2317.

[27] Premkumar K, Manikandan BV. Bat algorithm optimized fuzzy PD based speed controller for brushless direct current motor. Eng Science Tech 2016; 19: 818-840.

[28] Prabu MJ, Poongodi P, Premkumar K. Fuzzy supervised online coactive neuro-fuzzy inference system-based rotor position control of brushless DC motor. IET Power Electron 2016; 9: 2229-2239.

[29] Premkumar K, Manikandan BV. Fuzzy PID supervised online ANFIS based speed controller for brushless DC motor. Neurocomputing 2015; 157: 76-90.

[30] Sivarani TS, Jawhar SJ, Kumar CA, Premkumar K. Novel bacterial foraging-based ANFIS for speed control of matrix converter-fed industrial BLDC motors operated under low speed and high torque. Neural Comput Applic 2018; 29: 1411-1434.

[31] Premkumar K, Manikandan BV. Speed control of brushless DC motor using bat algorithm optimized adaptive neuro-fuzzy inference system. Appl Soft Comput 2015; 32: 403-419.

[32] Zhong R, Xu Y, Cao Y, Guo X, Hua W, Xu S, Sun W. Accurate model of switched reluctance motor based on indirect measurement method and least square support vector machine. IET Electr Power Appl 2016; 10: 916-922.

[33] Mudi RK, Pal NR. A robust self-tuning scheme for PI- and PD-type fuzzy controllers. IEEE T Fuzzy Syst 1999; 7: 2-16.